Wave Mode Conversion in Stiffened Cylindrical Shells With Periodic Axial Curvature

M. L. Accorsi
Department of Civil Engineering,
University of Connecticut,
Storrs, CT 06269-3037

M. S. Bennett
Electric Boat Corporation
Technology Development and Analysis,
Groton, CT 06340

Free wave propagation in periodically stiffened cylindrical shells is investigated using a periodic finite element method developed by the authors. The modification of longitudinal wave modes was a primary objective because of their long wavelengths and poor attenuation characteristics. Cylinder configurations that utilize periodic axial curvature are examined and are shown to have significantly more coupling between longitudinal and flexural wave modes than cylinders without axial curvature. This coupling significantly modifies the stop and pass band behavior.

In this paper, the periodic finite element method is first reviewed. The method is then applied to a one-dimensional periodic structure consisting of circular beam sections. The longitudinal/flexural wave mode conversion in this simple structure is illustrated. Finally, results for cylindrical shells with and without axial curvature are presented.

1 Introduction

Ribbed stiffened cylindrical shells are commonly used as primary structural components in numerous aerospace and naval applications. In these applications, the structural acoustics properties are often of primary concern. Assuming that the stiffeners are equally spaced, the wave propagation characteristics can be studied using specialized techniques for spatially periodic structures.

Free wave propagation in stiffened cylinders has been studied by several investigators. Hodges et al. [1] used a Rayleigh-Ritz technique to predict wave propagation in circumferentially stiffened cylinders. Their approach included two degrees of freedom to describe stiffener cross-sectional deformation. Their results demonstrate the importance of stiffener cross-sectional deformation even at low frequencies. Mead and Bardell [2] developed an exact solution technique for wave propagation in cylindrical shells with discrete circumferential stiffeners. Stiffener cross-sectional deformation, however, was not considered in their solution. These studies have been limited to circular cylindrical shells of constant radius.

Torsional wave mode coupling in a clad rod with multiple periodic interface corrugations has been investigated by Asfar and Hawwa [3] using an asymptotic approach. The ability to enhance the filtering characteristics of the waveguide by changing the properties of the interface corrugations is examined. In the present study, free wave propagation in stiffened cylindrical shells with periodic axial curvature are considered using a finite element method developed previously by the authors [4, 5]. The purpose of this configuration is to enhance the coupling between longitudinal and flexural wave modes. Attenuation of these waves due to material damping is inversely proportional to their wavelengths. Because of their long wavelength, longitudinal modes propagate over large distances with little attenuation. When these wave modes encounter a structural discontinuity, scattering occurs which often results in significant acoustic radiation. In the present study, coupling of longitudinal and flexural wave modes due to periodic axial curvature is examined and the associated stop and pass band characteristics are identified.

Before considering the cylindrical shell, a simpler structure consisting of periodic circular beam segments (Fig. 1) was analyzed to explore this concept. An exact solution for free wave propagation in this structure was developed. The results from the exact solution are compared to the finite element approach in order to provide independent verification of the finite element results.

2 Methodology

The exact solution and periodic finite element solution are first developed for analysis of wave propagation in the periodic circular beam structure. The transfer matrix approach developed by Signorelli and von Flotow [6] for one-dimensional periodic trusses is used for both. The finite element approach is then used to analyze axial wave propagation in axisymmetric stiffened cylinders as a function of circumferential wave number.

2.1 Wave Propagation in One-Dimensional Periodic Multi-Coupled Structures. A single circular beam section and the corresponding finite element model are shown in Fig. 2. For the exact solution, an exact dynamic stiffness matrix relating the left (L) and right (R) displacements and forces is found. For the finite element solution, the corresponding dynamic stiffness matrix is obtained by assembling the stiffness and mass matrices as $D = K - \omega^2 M$. The finite element model contains internal (I) degrees of freedom (DOF) in addition to the left and right DOF. For both solutions, the transfer matrix is obtained by partitioning the dynamic stiffness matrix D into left, right, and internal DOF. The exact solution is a special case where the internal DOF are absent. The partitioned equations are written as

$$\begin{bmatrix} D_{LL} & D_{LI} & D_{LR} \\ D_{IL} & D_{II} & D_{IR} \\ D_{RL} & D_{RI} & D_{RR} \end{bmatrix} \begin{Bmatrix} Q_L \\ Q_I \\ Q_R \end{Bmatrix} = \begin{Bmatrix} F_L \\ 0 \\ F_R \end{Bmatrix} \tag{1}$$

where the internal forces $F_I = 0$ for free wave propagation. The internal displacements Q_I are eliminated as follows

$$Q_I = -D_{II}^{-1}[D_{IL}Q_L + D_{IR}Q_R] \tag{2}$$

Substituting Eq. (2) into Eq. (1) yields

$$\begin{bmatrix} H_{LL} & H_{LR} \\ H_{RL} & H_{RR} \end{bmatrix} \begin{Bmatrix} Q_L \\ Q_R \end{Bmatrix} = \begin{Bmatrix} F_L \\ F_R \end{Bmatrix} \tag{3}$$

Contributed by the Technical Committee on Vibration and Sound for publication in the JOURNAL OF VIBRATION AND ACOUSTICS. Manuscript received April 1994; revised Aug. 1994. Associate Technical Editor: G. Koopmann.

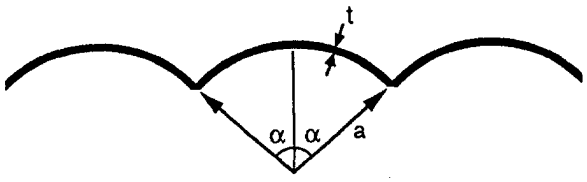

Fig. 1 Periodic circular beam structure

where

$$H_{mn} = D_{mn} - D_{mI}D_{II}^{-1}D_{In} \quad m, n = L, R \tag{4}$$

For the exact solution, the second term involving the internal DOF is absent and the result is simply $H_{mn} = D_{mn}$.

The transfer matrix T is obtained from Eq. (3, 4) by relating the right displacements and forces to those on the left

$$\begin{Bmatrix} Q_R \\ -F_R \end{Bmatrix} = T \begin{Bmatrix} Q_L \\ F_L \end{Bmatrix} \tag{5}$$

where

$$T = \begin{bmatrix} -H_{LR}^{-1}H_{LL} & H_{LR}^{-1} \\ H_{RR}H_{LR}^{-1}H_{LL} - H_{RL} & -H_{RR}H_{LR}^{-1} \end{bmatrix} \tag{6}$$

The wave propagation characteristics of a periodic structure are given by Floquet's theorem. For the one-dimensional structure considered, Floquet's theorem is written as

$$\begin{Bmatrix} Q_R \\ -F_R \end{Bmatrix} = e^{\mu} \begin{Bmatrix} Q_L \\ F_L \end{Bmatrix} \tag{7}$$

where μ is the propagation constant. Subtracting Eq. (7) from Eq. (5) results in the following linear eigenvalue problem for determination of the propagation constants.

$$[T - e^{\mu}I] \begin{Bmatrix} Q_L \\ F_L \end{Bmatrix} = 0 \tag{8}$$

The propagation constants are frequency dependent and, in general, are complex. The real part of the propagation constant μ_R, called the attenuation constant, gives the amplitude decay

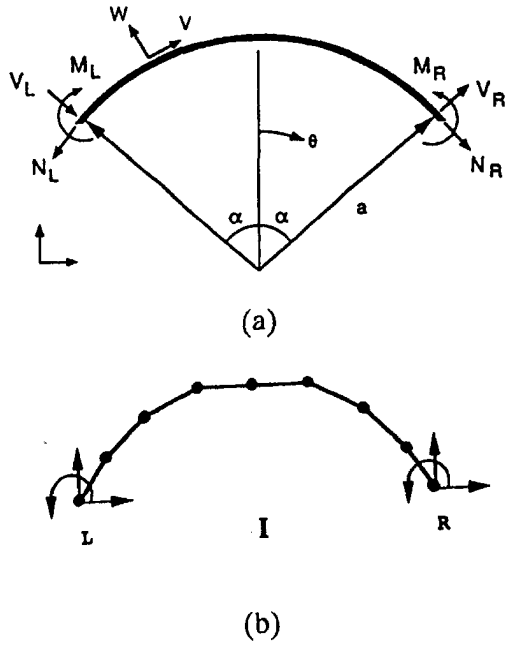

Fig. 2 (a) Circular beam, (b) FE model

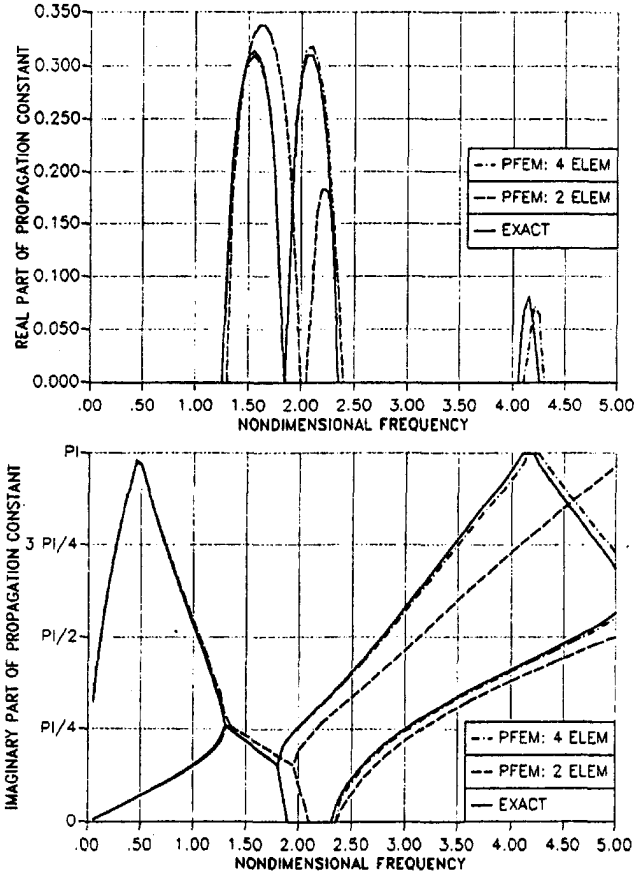

Fig. 3 Comparison of PFEM and exact solution for α = 10 deg

over one periodic spacing. The imaginary part μ_I, known as the phase constant, gives the phase change of the travelling wave over one periodic spacing.

2.2 Exact Solution for Periodic Circular Beam Structure. In this section the exact dynamic stiffness matrix D for the circular beam structure will be found. The governing equations for harmonic vibration of a circular beam are given by

$$\frac{d^2v}{d\theta^2} + \frac{dw}{d\theta} + \Omega^2 v = 0 \tag{9}$$

$$\frac{dv}{d\theta} + w + \beta^2 \frac{d^4w}{d\theta^4} - \Omega^2 w = 0 \tag{10}$$

$$N_\theta = \frac{Eh}{a}\left(\frac{dv}{d\theta} + w\right) \quad M_\theta = \frac{Et^3}{12a^2}\frac{d^2w}{d\theta^2}$$

$$Q_\theta = -\frac{Et^3}{12a^3}\frac{d^3w}{d\theta^3} \tag{11}$$

where

$$c^2 = \frac{E}{\rho} \quad \beta^2 = \frac{t^2}{12a^2} \quad \Omega^2 = \frac{a^2\omega^2}{c^2}$$

and v and w are the tangential and radial displacements, respectively. Equations (9) and (10) are a special case of the equations of motion for a cylindrical shell where there is no axial (z) dependence. Seeking a solution in the form

$$v(\theta) = Ve^{ik\theta} \quad w(\theta) = We^{ik\theta} \tag{12}$$

leads to the following sixth order polynomial for k

$$k^6 - \Omega^2 k^4 - \frac{\Omega^2}{\beta^2} k^2 + \frac{\Omega^2}{\beta^2}(\Omega^2 - 1) = 0 \qquad (13)$$

The roots of Eq. (13) are found by substituting $s = k^2$ and using the exact solution for the roots of a cubic equation in s. The following relationship between the amplitudes of the two displacement components is also found

$$V_j = \frac{-ik_j W_j}{(\Omega^2 - k_j^2)} \quad j = 1, 6 \qquad (14)$$

This relation is used to eliminate the tangential displacement terms V_j from the formulation.

The dynamic stiffness matrix is found by relating end displacements Q to end forces F. First the displacements at the left and right ends of the circular section are prescribed. This is written as

$$[R]\{W\} = \{Q\} \qquad (15)$$

where

$$\{Q\}^T = [v_L, w_L, \phi_L, v_R, w_R, \phi_R]$$
$$\{W\}^T = [W_1, W_2, W_3, W_4, W_5, W_6] \qquad (16)$$

and $\phi = (1/a)(dw/d\theta)$ is the end rotation and R is a known matrix derived from the solution given in Eq. (12). Next the end forces are expressed in terms of W_j

$$\{F\} = [S]\{W\} \qquad (17)$$

where

$$\{F\}^T = [N_L, V_L, M_L, N_R, V_R, M_R] \qquad (18)$$

and S is a known matrix derived from Eq. (11), (12) and (14). Substituting Eq. (15) into Eq. (17) gives the following expression for the dynamic stiffness matrix d.

$$[d] = [S][R]^{-1} \qquad (19)$$

The quantities in Eq. (19) are in the local polar coordinate system shown in Fig. 2(*a*). The global dynamic stiffness matrix is $D = \lambda^T d \lambda$ where λ is a rotation matrix relating the local polar coordinate system [Fig. 2(*a*)] to the global system [Fig. 2(*b*)] at the left and right ends. Although the solution is not written explicitly in closed form, the solution is considered exact since no numerical approximations are used.

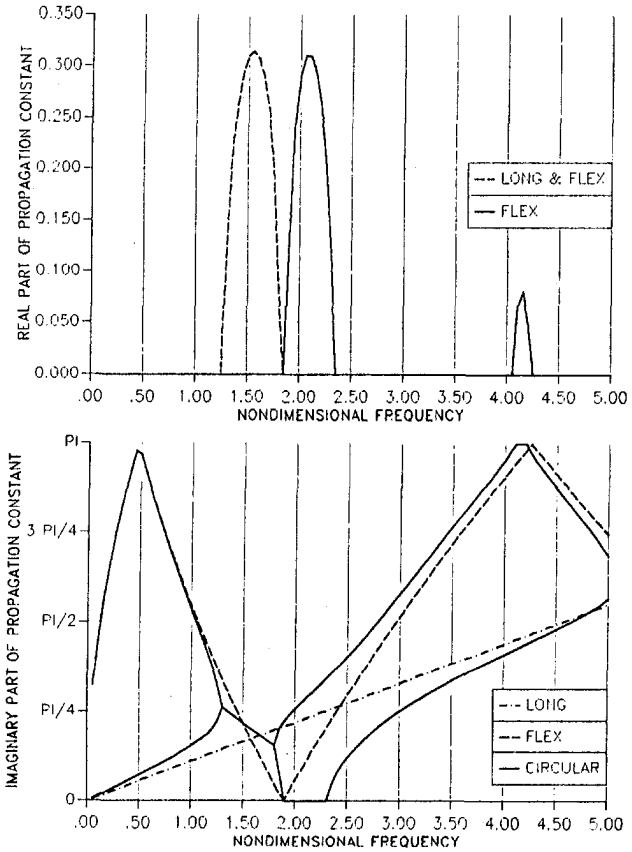

Fig. 4 Propagation constants for α = 10 deg

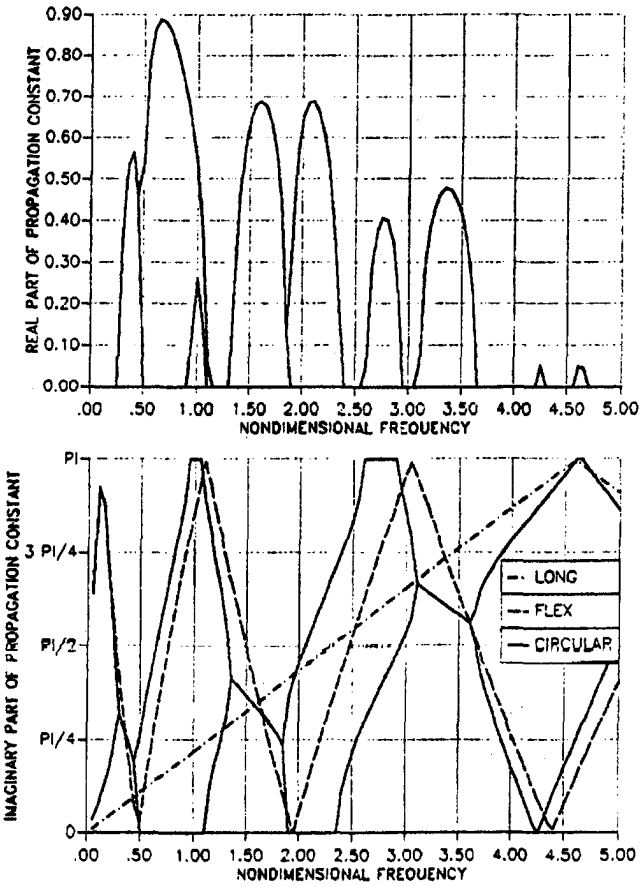

Fig. 5 Propagation constants for α = 20 deg

2.3 Axial Wave Propagation in Axisymmetric Stiffened Cylindrical Shells. For axisymmetric stiffened cylinders, the one-dimensional finite element formulation can be used to determine axial propagation constants μ_z as a function of circumferential wave number n (Bennett and Accorsi, 1993). In this case, the assembled stiffness and mass matrices for the axisymmetric model are functions of n, and the dynamic stiffness matrix is written as $D(n) = K(n) - \omega^2 M(n)$.

3 Results

Propagation constants for the periodic circular beam structure were evaluated using the exact solution and finite element approach. These results can be best understood by comparison with an infinite straight beam with longitudinal and flexural wave modes. For a straight beam, there are two propagating longitudinal waves, two propagating flexural waves, and two nonpropagating flexural waves at all frequencies. Each wave pair corresponds to equal left and right waves.

Propagation constants for the circular beam structure were evaluated as a function of nondimensional frequency ($0 \leq \Omega \leq 5$) using the material properties of steel and a thickness to

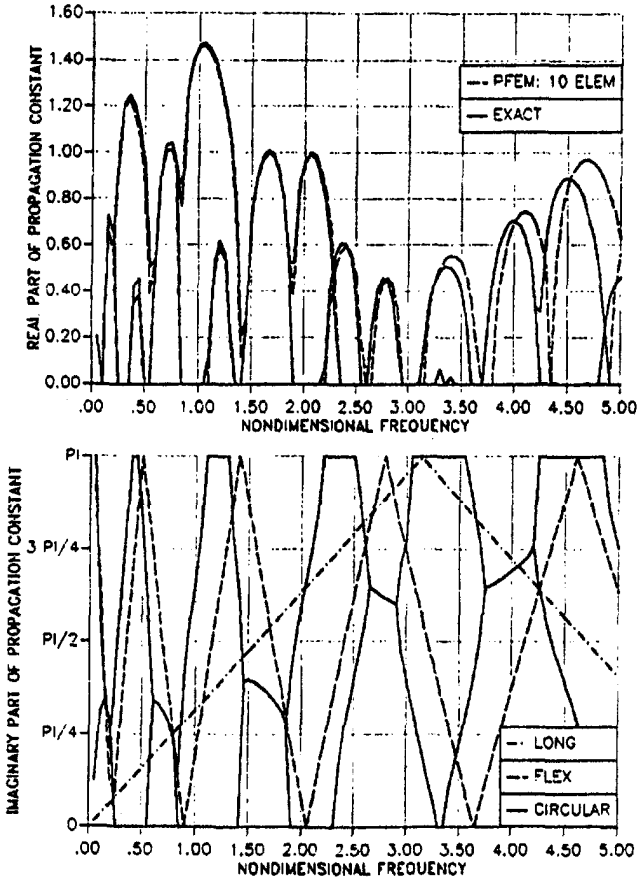

Fig. 6 Propagation constants for $\alpha = 30$ deg

radius ratio $t/a = 1/50$. Results are given for a subtended angle of $\alpha = 10$ deg, 20 deg, and 30 deg (see Fig. 1). For these properties, the nonpropagating flexural waves remained virtually unchanged from the straight beam results. However, the propagating longitudinal and flexural modes become coupled in certain frequencies ranges resulting in new stop bands (nonzero μ_R) that are not present in the straight beam case.

Propagation constants predicted by the periodic finite element method (PFEM) and exact solution are shown for $\alpha = 10$ deg, in Fig. 3. For the real part, only the new stop bands caused by the periodic circular geometry are shown. Two approximations apply to the PFEM. First, polynomial shape functions are used to generate the stiffness and mass matrices, and secondly, the

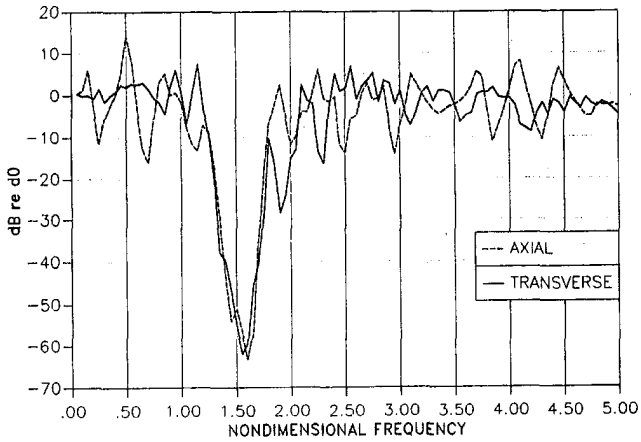

Fig. 7 Harmonic analysis of periodic circular and straight beam

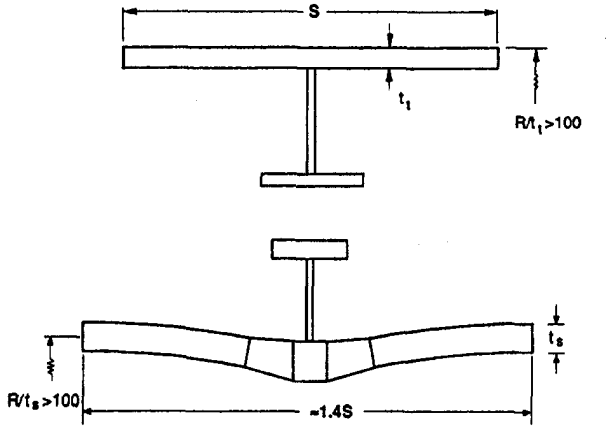

Fig. 8 Axisymmetric stiffened cylindrical shells

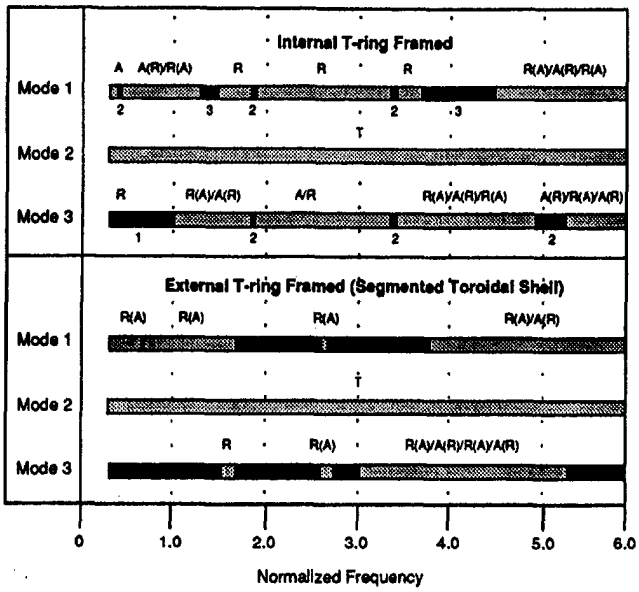

Fig. 9 Stop and pass bands for $n = 0$

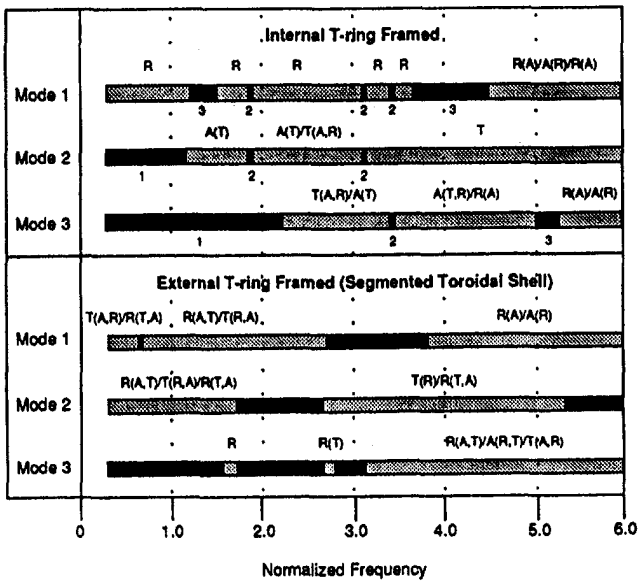

Fig. 10 Stop and pass bands for $n = 2$

circular geometry is approximated by facetted straight beam elements. The comparison is shown using only two and four elements. For two elements, the PFEM results agree poorly with the exact solution over the entire frequency range. For four elements, the PFEM results agree well with the exact solution for low frequencies but deviate at higher frequencies. These results demonstrate the validity of the PFEM when adequate model refinement is maintained.

The real and imaginary parts of the propagation constants predicted by the exact solution are shown in Fig. 4 for $\alpha = 10$ deg. For the imaginary part, the propagating longitudinal and flexural modes for a straight beam (dashed lines) are shown for comparison with the periodic circular beam (solid lines). For the straight beam, the wave numbers k are plotted as principal values of the phase constant ($0 \leq \mu_l \leq \pi$) where $\mu_l = ikl$ and l is the length of the periodic spacing. The motion associated with each wave mode for the circular periodic structure can be determined from the eigenvectors of Eq. (8). The primary motion associated with the new stop bands have been labelled in Fig. 4. The first new stop band ($1.25 \leq \Omega \leq 1.85$) corresponds to both longitudinal and flexural motions with the two propagation constants being complex conjugates. In the second stop band ($1.85 \leq \Omega \leq 2.35$), the flexural propagation constant is real and the longitudinal propagation constant is imaginary. In the third stop band ($4.05 \leq \Omega \leq 4.25$), the flexural propagation constant is complex (with $\mu_l = \pi$) and the longitudinal propagation constant is imaginary.

The propagation constants for a circular beam with angles $\alpha = 20$ deg and 30 deg are shown in Figs. 5 and 6, respectively. The general behavior described previously is seen in these results; however, the coupling of the longitudinal and flexural wave modes becomes much stronger resulting in more new stop bands and greater deviation from the straight beam case. A comparison between the PFEM using 10 elements and the exact solution is shown in Fig. 6 for the real part of the propagation constant. Good agreement is achieved at low frequencies, but deviation occurs at higher frequencies indicating the need for further model refinement.

A harmonic analysis was performed on two finite beams consisting of twenty straight and circular periodic units. Each model was loaded separately by an axial and transverse harmonic force at the left end, and the axial and transverse displacement at the right end was calculated. The axial and transverse displacements for the periodic circular beam for $\alpha = 10$ deg at the right end, d_{10}, are nondimensionalized by the corresponding displacements for the straight beam ($\alpha = 0$ deg), d_0, in order to compare their behavior. A loss factor of $\eta = 0.01$ was used in the calculation. A plot of nondimensional displacement (dB re d_0) versus frequency is shown in Fig. 7 for axial and transverse loading. Due to the finite length of the beams, resonances are present in the frequency response. The resonances for the periodic beam are different than the straight beam and appear, respectively, as local peaks and dips due to the nondimensionalization. The large dip in both the axial and transverse harmonic response of the periodic circular beam occurs in the first new stop band. In the second and third stop bands the dips are less pronounced. Outside of these stop bands, where the propagation constants for the undamped structure are purely imaginary, the mean response of the two beams is about the same. Therefore, the wave mode coupling does not appear to significantly affect the dissipation in these regions.

3.1 Axisymmetric Stiffened Cylindrical Shells. The two cylindrical shells considered in this study are shown in Fig. 8. The first is a conventional configuration (constant radius) using an internal T stiffener. The second configuration (segmented toroid) incorporates periodic axial curvature and an external T stiffener. Results are shown for circumferential wavenumbers $n = 0$ and $n = 2$ in Figs. 9 and 10, respectively.

To simplify presentation of the results, only the locations of stop bands (black fill) and pass bands (grey shading) are given. The dominant wave mode is indicated by an A, R, or T corresponding to axial, radial, or tangential displacement, respectively. A letter in parentheses indicates appreciable motion in a second direction, and a slash indicates conversion of the maximum displacement from one direction to another.

For the conventional configuration, three types of stop bands can be identified. The first type occurs below the cut-off frequency of the cylinder and is not associated with axial periodicity of the cylinder (identified in Figs. 9 and 10 by a 1 below the stop band). The second type is primarily associated with stiffener resonances (identified in Figs. 9 and 10 by a 2). These appear as small, very discrete stop bands. The third type occurs when the structural half wavelength (or its multiples) equal the stiffener spacing (identified in Figs. 9 and 10 by a 3). From an acoustic design viewpoint, the third type of stop band are of primary interest since they are broadband and can be tuned to various frequency ranges by changing the stiffener spacing.

Comparison of the results for the conventional configuration and segmented toroid show very different behavior. The segmented toroid has significantly more stop band behavior due to coupling of the radial and axial wave modes. This behavior is analogous to the results for the circular beam structure presented in the previous section.

4 Conclusions

Wave propagation in structures with periodic axial curvature has been examined using a simple circular beam structure and segmented toroidal shell. Comparison of an exact solution with the periodic finite element method for the circular beam structure showed excellent agreement which provides verification of the finite element procedure. The periodic axial curvature causes coupling between the longitudinal and flexural modes resulting in new stop bands that are not present in a straight beam. Similar behavior was observed in the segmented toroidal shell. A harmonic analysis of a finite structure demonstrates that the stop band behavior is preserved in a finite structure, but no significant additional dissipation occurs outside of these stop bands due to wave mode coupling.

5 Acknowledgment

Funding for this work was provided by the Independent Research and Development Program at Electric Boat Corporation and the State of Connecticut Department of Economic Development.

6 References

1 Hodges, C., Power, J., and Woodhouse, J., 1985, "The Low Frequency Vibration of a Ribbed Cylinder, Part 1: Theory," *Journal of Sound and Vibration,* Vol. 101, pp. 219–235.

2 Mead, D., and Bardell, N., 1986, "Free Vibration of a Thin Cylindrical Shell with Periodic Circumferential Stiffeners," *Journal of Sound and Vibration,* Vol. 115, pp. 499–520.

3 Asfar, O. R., and Hawwa, M. A., 1993, "Torsional Mode Coupling and Filtering in a Composite Waveguide with Multiperiodic Interface Corrugations," *J. Acoust. Soc. Am.,* Vol. 93, pp. 2468–2473.

4 Accorsi, M., and Bennett, M., 1991, "A Finite Element Based Method for the Analysis of Free Wave Propagation in Stiffened Cylinders," *Journal of Sound and Vibration,* Vol. 148, pp. 279–292.

5 Bennett, M., and Accorsi, M., 1993, "Free Wave Propagation in Periodically Ring Stiffened Cylindrical Shells," *Journal of Sound and Vibration,* Vol. 171, pp. 49–66.

6 Signorelli, J., and von Flotow, A., 1988, "Wave Propagation, Power Flow, and Resonance in a Truss Beam," *Journal of Sound and Vibration,* Vol. 126, pp. 127–144.